

**Diamagnetic and paramagnetic shifts in self-assembled InAs lateral quantum dot molecules**Xinran Zhou,<sup>1</sup> Miquel Royo,<sup>2</sup> Weiwen Liu,<sup>1</sup> Jihoon H. Lee,<sup>3,4</sup> Gregory J. Salamo,<sup>4</sup> Juan I. Climente,<sup>2</sup> and Matthew F. Doty<sup>1,\*</sup><sup>1</sup>*Department of Materials Science and Engineering, University of Delaware, Newark, Delaware 19716, USA*<sup>2</sup>*Departament de Química Física i Analítica, Universitat Jaume I, E-12080 Castello, Spain*<sup>3</sup>*School of Electronics and Information, Kwangwoon University, Nowon-gu, Seoul 139-701, South Korea*<sup>4</sup>*Institute of Nanoscale Science and Engineering, University of Arkansas, Fayetteville, Arkansas 72701, USA*

(Received 5 November 2014; revised manuscript received 28 April 2015; published 19 May 2015)

We uncover the underlying physics that explains the energy shifts of discrete states of individual InAs lateral quantum dot molecules (LQDMs) as a function of magnetic fields applied in the Faraday geometry. We observe that ground states of the LQDM exhibit a diamagnetic shift while excited states exhibit a paramagnetic shift. We explain the physical origin of the transition between these two behaviors by analyzing the molecular exciton states with effective mass calculations. We find that charge carriers in delocalized molecular states can become localized in single QDs with increasing magnetic field. We further show that the net effects of broken symmetry of the molecule and Coulomb correlation lead to the paramagnetic response.

DOI: [10.1103/PhysRevB.91.205427](https://doi.org/10.1103/PhysRevB.91.205427)

PACS number(s): 78.67.Hc, 71.35.Ji, 78.20.Ls, 78.55.Cr

**I. INTRODUCTION**

Self-assembled quantum dots (QDs) are of great interest for both fundamental studies of confined electronic states and applications in next-generation optoelectronic devices [1–3]. Molecules composed of two or more QDs are analogous to “natural” molecules in that delocalized molecular states with unique properties can be created by coherent tunneling between the “atomic” constituents [4–15]. Unlike natural molecules, the molecular states of quantum dot molecules (QDMs) can be tailored during growth or manipulated *in situ* with applied electric, magnetic, and optical fields. These properties make QDMs particularly interesting as components of future solid state optoelectronic devices.

Lateral QDMs (LQDMs) are composed of two quantum dots aligned side-by-side on the growth surface. Although the tunnel coupling in LQDMs is typically weaker than in vertical QDMs (dots stacked along the growth direction), LQDMs are compatible with the creation of devices that simultaneously manipulate interdot coupling and charge occupancy by applying electric fields in two dimensions [16,17]. Our previous spectroscopy and analysis of single LQDMs has revealed distinct spectral patterns that are characteristic of LQDMs with nearly degenerate and nondegenerate “atomic” constituents [15]. These results agree with prior computational and experimental work that suggests the existence of delocalized molecular states under certain conditions [18–23]. Here we report the observation of diamagnetic shifts for carriers confined in the ground state of LQDMs and large paramagnetic shifts for carriers confined in the first excited state. We use effective mass models to explain the physical origins of this transition and show that the delocalized molecular states in the LQDMs are localized to single QDs by the magnetic field, substantially changing both the Coulomb interaction strengths and angular momentum of the charges in the LQDMs. As a result, the broken symmetry of the LQDM, relative to the near-circular symmetry of a single QD, enhances the paramagnetic response of the excited states. The results reveal new opportunities for “molecular engineering” in the solid state.

agnetic response of the excited states. The results reveal new opportunities for “molecular engineering” in the solid state.

**II. EXPERIMENTAL**

The LQDMs we study are grown from single dome-shaped QDs that are partially covered and annealed. Anisotropic diffusion along the reconstructed [0 1 –1] crystal axis drives the formation of side-by-side InAs quantum dots connected by an In-rich basin [24]. The LQDMs are grown in an *n*-doped Schottky diode configuration and patterned with electrodes that apply an electric field along the growth direction to control the total charge occupancy of the LQDM.

We use magneto-optical spectroscopy to study both ground and excited states of individual LQDMs. The LQDM sample was held in an Advanced Research Systems DMX-20 cryostat for ensemble measurements and moved into a liquid-helium-cooled cryostat with a superconducting solenoid for measurement of PL from individual LQDMs as a function of magnetic field. The LQDMs are cooled to 8 K and subject to a magnetic field of up to 6 T in the Faraday geometry; i.e., the magnetic field is parallel to the optical axis and growth direction, but perpendicular to the molecular axis. The ensemble PL is excited by a Ti:sapphire laser at 860 nm with power density ranging from 71 W/cm<sup>2</sup> to 5 kW/cm<sup>2</sup>. The PL signal is resolved with a 0.75 m spectrometer equipped with a liquid-nitrogen-cooled charge-coupled device (CCD) camera using a diffraction grating with 150 grooves/mm. The discrete PL lines from single LQDMs are excited by a diode laser at 890 nm with power density of 200 W/cm<sup>2</sup> and resolved with a CCD using a diffraction grating with 1200 grooves/mm.

Figure 1(b) shows the photoluminescence (PL) of an ensemble of LQDMs. Four distinct peaks, corresponding to emission from the ground states (GS) and first-through-third excited states (ES1-ES3) are observed at high excitation power. We note that the intensity of the GS relative to the ES is influenced by the wavelength sensitivity of our Si CCD camera. Multipeak fitting of the ensemble PL reveals the energy separation between each energy shell; the GS and ES1 are typically separated by about 50 meV.

\*doty@udel.edu

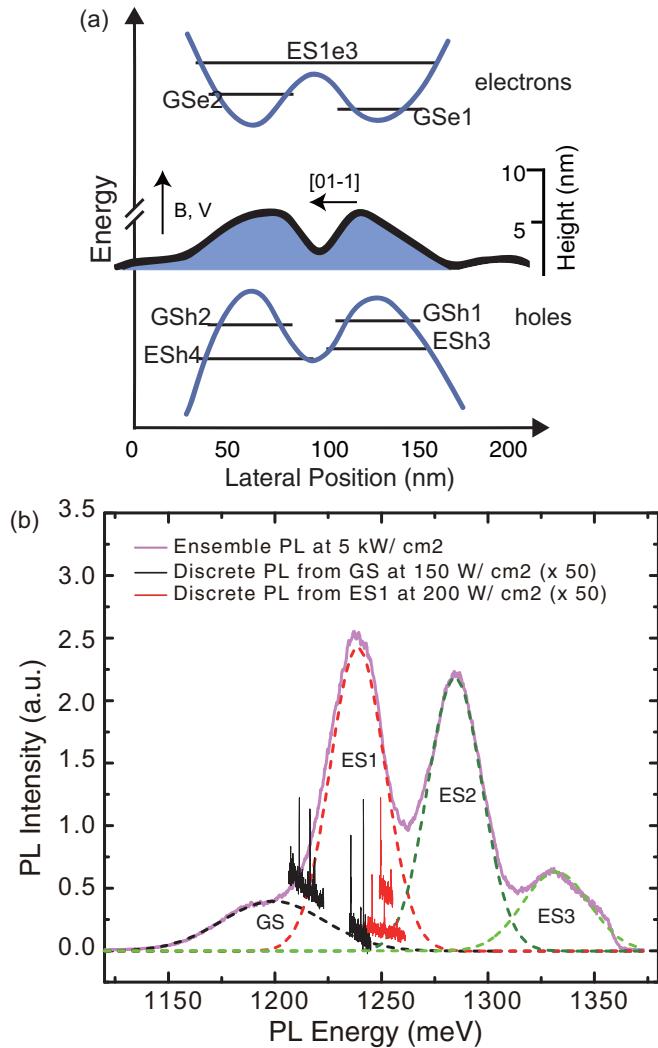


FIG. 1. (Color online) (a) Schematic band diagram of a single LQDM. The middle inset shows the cross-sectional profile of a single LQDM with arrows denoting the molecular axis and the direction of applied electric and magnetic fields. (b) PL from LQDM ensemble (blue), single LQDM GSs (black), and single LQDM ES1s (red) measured in flat-band conditions with zero magnetic field. The ensemble PL is fitted by four Gaussian curves (dashed lines) to identify four PL energy shells.

### III. ENERGY SHELL STRUCTURES OF LQDMs

As reported previously, the ground states of confined electrons and holes of LQDMs are localized in individual QDs [14,15]. The first excited state for holes is largely localized, but the first excited state of electrons is delocalized over the LQDM. This electronic structure is schematically depicted in Fig. 1(a) and numerical calculations of the spatial extent of the carrier electronic density are presented in Fig. 4.

Previous work on this LQDM sample establishes that all of the observed PL lines originate in LQDMs rather than single QDs [14,15]. AFM images for an uncapped reference LQDM sample indicate that over 90% of the QD complexes are composed of two laterally aligned QDs. In the case in which a single QD or clusters with more than two QDs are evolved, the

PL energies of those QD configurations will be significantly different from the energies of two-QD LQDMs because the total amount of InAs in the QD complex is conserved during the evolution from single to double to multiple QDs. Because the size of the QD, limited by the volume of available InAs, determines the emission energy, we can rule out the possibility that PL in the spectral range we studied could have originated in structures other than “diatomic” LQDMs.

Our prior work also establishes the existence of delocalized ES1 states for all LQDMs in this sample [14,15]. Although the degree of degeneracy of different LQDMs varies with the geometry and material composition of each LQDM, previous experimental and theoretical studies of the ES1 states of our LQDMs reveal that the existence of delocalized excited electron states is universal, regardless of the degeneracy of the neighboring QDs. The calculated exciton charge densities of LQDMs shown in Fig. 7(b) also indicate that the delocalization of electrons still exists even if the interdot distance and energy difference are large ( $\Delta E = 8$  meV,  $d = 38$  nm).

The black and red lines in Fig. 1(b) show discrete PL lines obtained from individual LQDMs. The time-integrated measurement approach allows the emission from higher-energy shells to be measured even at relatively low excitation power. The intensity of different PL peaks corresponds to the probability that the corresponding energy shell is occupied. We focus on the GS PL lines with higher-than-average energies to improve detection efficiency with our Si-based CCD. Emission from the GS and ES1 is easily distinguished by observing characteristic applied voltage and laser power dependence trends in the PL data [14,15]. A typical result for this power-dependent measurement is shown in Fig. 2(a). With increasing laser power density, the increase of the PL intensities of the three peaks with low energy [marked as G1, G2, and G3; see Fig. 2(b)] rise sublinearly with a change in slope at a laser power density of approximately  $125$  W/cm<sup>2</sup>. In contrast, the intensities of peaks in the high-energy side [see Fig. 2(c)] increase superlinearly with increasing laser power. The different trends of these two groups of lines indicate that PL lines G1, G2, and G3 are emitted from the ground shell of the LQDMs (GS) while E1, E2, and E3 are from the first excited shell (ES1) [14]. We have also noticed that the Stark shift of PL lines in different shells varies. These two methods allow us to assign PL lines to specific energy shells.

### IV. ENERGY SHIFTS OF GS AND ES1 SHELLS UNDER MAGNETIC FIELDS

Figure 3(a) shows the typical magnetic field dependence of PL emission from the GS and ES1, measured on two different LQDMs. The GS exhibits a 0.6 meV blueshift as the magnetic field is increased to 6 T and a Zeeman splitting that reaches 0.3 meV. Over the same range of magnetic field ES1 exhibits a strong redshift (about 3.5 meV). Although the lines broaden slightly, no Zeeman splitting in the ES1 PL is observed within the range of magnetic fields studied. The continuous and smooth energy shifts and the full PL spectral maps (not shown) confirm that the number of charges in each LQDM does not change as a function of magnetic field.

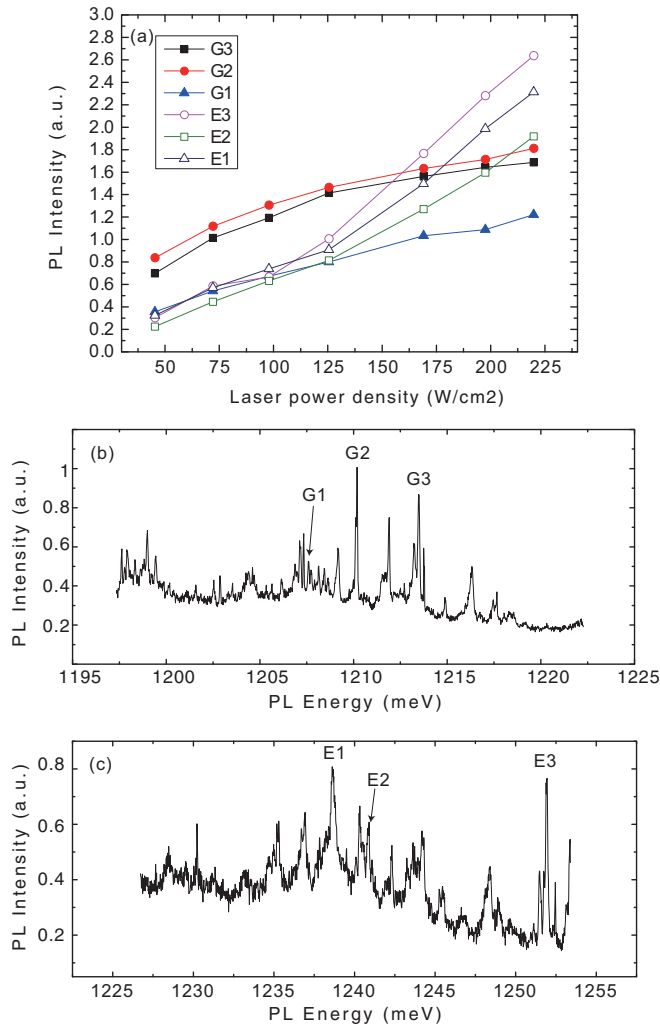


FIG. 2. (Color online) (a) Dependence of photoluminescence intensity of discrete spectral lines emitted from LQDMs excited by a laser with power ranging from 50 to 225 W/cm<sup>2</sup>. The PL peak labels correspond to discrete ground (b) or excited (c) states evident in the line spectra.

The PL energy of QD ground states as a function of magnetic field is typically fitted with an equation of the form

$$E_{pl}(B) = E_{pl}(0) \pm b_{ex}B + a_{ex}B^2, \quad (1)$$

where  $E_{pl}(0)$  is the PL energy at 0 T,  $b_{ex}$  is the linear coefficient, and  $a_{ex}$  is the quadratic coefficient. Typically, in GS emissions, the linear term  $\pm b_{ex}B$  corresponds to the Zeeman splitting and  $b_{ex}$  is given by  $1/2\mu_B g_{ex}$ , where  $g_{ex}$  is the exciton  $g$  factor and  $\mu_B$  is the Bohr magneton. The quadratic term  $a_{ex}B^2$  typically comes from the geometric confinement caused by the magnetic field and is referred to as the diamagnetic shift. By fitting the GS data in Fig. 3(a) with this equation, we are able to extract the linear and quadratic coefficients in a phenomenological way. For the PL emission of ES1, we set  $b_{ex}$  to zero because no Zeeman splitting is observed. In most of the ES1 PL lines no Zeeman splitting or broadening is observed. However, PL peak broadening with increasing magnetic field has been observed in several cases. This broadening could be related to Zeeman splitting that

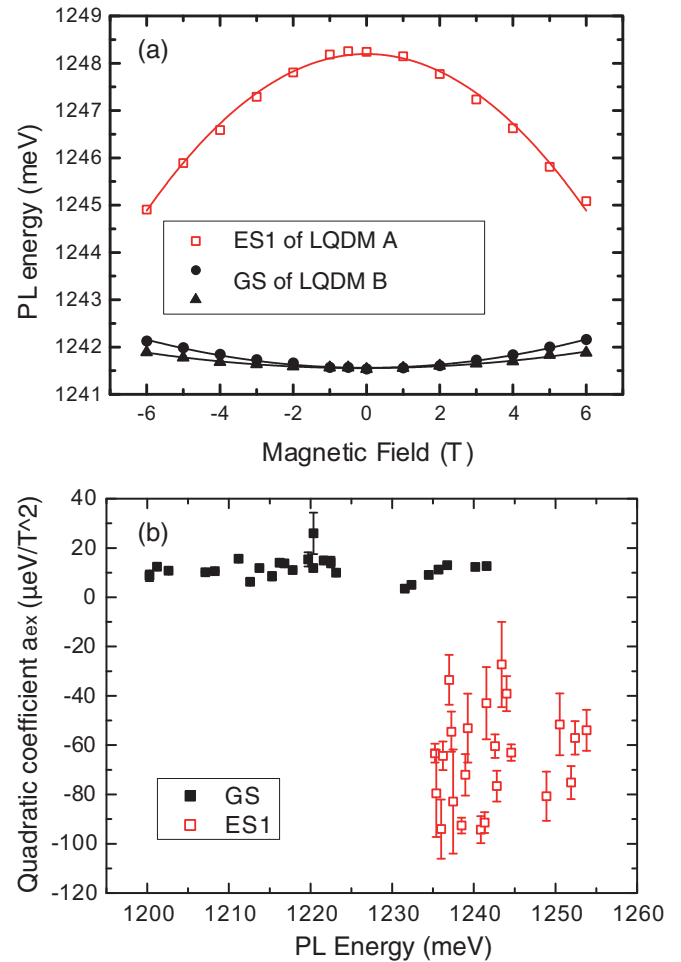


FIG. 3. (Color online) (a) Energies of typical PL lines (GS, ES1) from two representative LQDMs as a function of magnetic field. (b) Diamagnetic coefficients for discrete PL lines from different energy shells of LQDMs as a function of PL energy.

is below our spectral resolution. We do not have conclusive measurements or theory to address this point further. The fit value for  $a_{ex}$  is negative, in contrast to the positive value for the ground state PL. This negative  $a_{ex}$  quantifies the paramagnetic shift for the excited state that is evident in Fig. 3(a).

We apply the same fit to the magnetic-field-dependent PL data of 25 distinct ground states and 23 distinct excited states of LQDMs. The values of  $a_{ex}$  returned by these fits are plotted in Fig. 3(b) as a function of PL energy. The average  $a_{ex}$  for GS PL (solid symbols) is  $11.73 \mu\text{eV}/\text{T}^2$  and the standard deviation is  $4.27 \mu\text{eV}/\text{T}^2$ . This value is consistent with the diamagnetic coefficient observed for ground states of single InAs QDs and vertically stacked QDMs [25,26]. The average value of  $a_{ex}$  for ES1 PL (open symbols), on the other hand, is  $-65.36 \mu\text{eV}/\text{T}^2$ , approximately 6 times larger in magnitude and opposite in sign. The standard deviation of  $a_{ex}$  in ES1 is  $19.59 \mu\text{eV}/\text{T}^2$ . Redshifts of the excited state PL of single QDs, which have been well understood, originate in the circular symmetry of the single QD [27,28]. Unlike the well-localized charges in the GS, the wave function for charges in ES1 is better compared to the wave function for charges in quantum dots elongated along a certain lattice direction because of anisotropic growth [29].

The delocalized ES1 states in LQDMs do not have the circular symmetry of individual QDs and hence a new mechanism is required to explain the observed paramagnetic shifts.

## V. THEORETICAL EXPLANATIONS

We now use single-band two-dimensional effective mass calculations to explain the physical origin of the pronounced redshift in the ES1 PL. We consider an exciton confined in the LQDM, described by the Hamiltonian  $H_X = H_e + H_h + V_{eh}$ . Here  $V_{eh}$  is the Coulomb interaction between electron and hole and  $H_e$  and  $H_h$  are the electron and hole single-particle Hamiltonians:

$$H_i = \frac{\mathbf{p}^2}{2m_i^*} - \frac{q_i B}{2m_i^*} L_z + \frac{(q_i B)^2}{8m_i^*} (x^2 + y^2) + V_c^i, \quad (2)$$

where  $m_i^*$  is the effective mass of the electron ( $i = e$ ) or hole ( $i = h$ ),  $q_i$  is the charge ( $q_e = -1, q_h = 1$ ),  $B$  is the vertical magnetic field,  $L_z = (xp_y - yp_x)$  the azimuthal angular momentum, and  $V_c^i$  the confining potential. Hereafter we refer to the linear-in- $B$  term of  $H_i$  as  $H_i^{B1}$ , and to the quadratic-in- $B$  term as  $H_i^{B2}$ . We neglect the Zeeman effect, which is not relevant for determining the redshift of ES1. We use the same material parameters and confining potential that previously showed good agreement with experimental measurements of a nearly degenerate LQDM from the same sample at zero magnetic field [15].

The single-particle Hamiltonian [Eq. (2)] is integrated using three-point finite differences on a two-dimensional grid. The magnetic field is implemented with the symmetric gauge. Gauge invariance of the finite-difference discretization was checked by comparison with an alternative discretization formalism that averages the wave function in the  $B^2$  term, as done, e.g., in Ref. [30]. The exciton Hamiltonian  $H_X$  is solved using a configuration interaction (CI) method in the basis formed from the 36 (48) lowest electron (hole) spin-orbitals. Coulomb integrals are obtained using the Fourier transform convolution theorem. The CI matrix is built and diagonalized using the CItool software [33]. The resulting exciton states are of the form  $\Psi(\mathbf{r}_e, \mathbf{r}_h) = \sum c_{ij} \phi_i(\mathbf{r}_e) \phi_j(\mathbf{r}_h)$ , where  $\phi_n$  denotes a single-particle spin-orbital.

The emission intensity is estimated within the dipolar approximation as proportional to the square of the electron-hole overlap, considering holes as complex-conjugated electrons,

$$I \propto |S_{eh}|^2 = \left| \sum_{ij} c_{ij} \int \phi_i(\mathbf{r}_e)^* \phi_j(\mathbf{r}_h)^* \delta(\mathbf{r}_e - \mathbf{r}_h) d\mathbf{r}_e d\mathbf{r}_h \right|^2. \quad (3)$$

We note that considering a single exciton in excited states neglects quantitative corrections that may arise for ES1 PL due to the presence of additional excitons forming a closed shell in the lower-energy states. In single QDs such corrections have been estimated to be no more than 1 meV [31].

We first compute the excitonic electron and hole charge densities in the two ground states (GS1 and GS2) and the first excited state (ES1). As shown in Fig. 4, at  $B = 0$  T the GS charge densities of both electrons (left panels) and holes (right panels) are localized in individual QDs. For the first excited

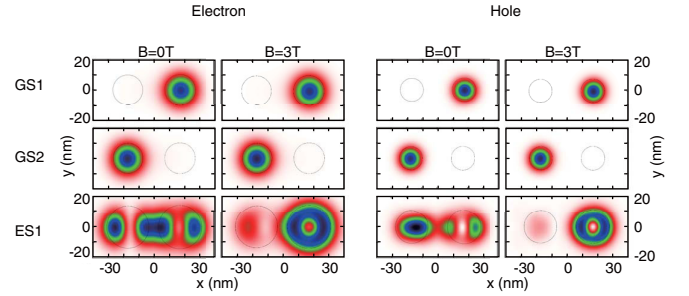


FIG. 4. (Color online) Electron (left panels) and hole (right panels) charge densities corresponding to the three relevant exciton states at  $B = 0$  T and  $B = 3$  T. Dashed line circumferences depict the characteristic length of the harmonic oscillators defining each QD calculated for the electron and hole states with the largest contribution in the exciton wave function.

state, the hole is also mainly localized inside one QD (left dot), but the electron is clearly delocalized over the whole LQDM, forming a molecular orbital. This picture is consistent with that inferred in previous experiments on LQDMs [14]. When the magnetic field is switched on,  $B = 3$  T, the GS charges remain largely unaffected. By contrast, the excited electron becomes trapped into the right QD, and the hole follows behind bound by Coulomb interaction. In other words, the magnetic field turns off the molecular character of the excited state.

Next, we compute the exciton emission spectrum as a function of  $B$ . The result is shown in Fig. 5(a). Black dots are used for emission from the two GS, red dots for emission from ES1, and gray dots for other transitions (e.g., transitions involving

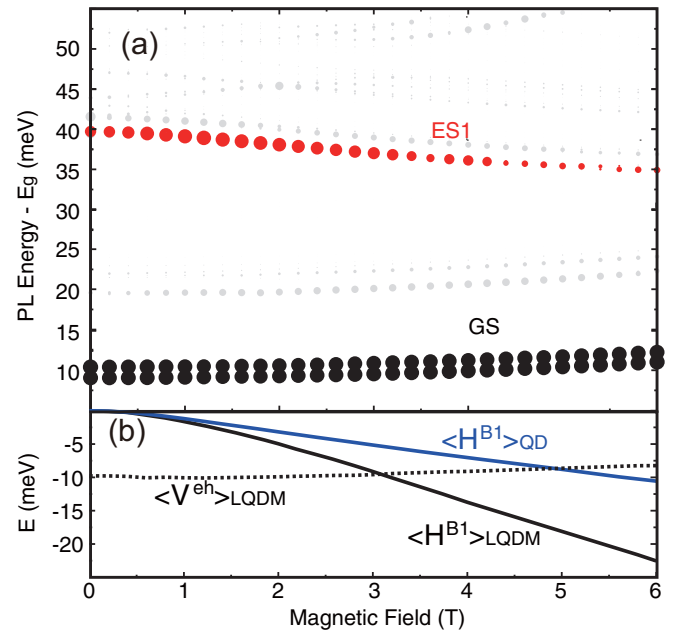


FIG. 5. (Color online) (a) Exciton emission spectrum as a function of magnetic field. Black dots are used for GS1 and GS2, red dots for ES1, and gray dots for other nonrelevant exciton states. The size of the dots is proportional to the optical intensity. (b) The expectation values of Coulomb interaction (dashed) and linear-in- $B$  single-particle terms for a LQDM (solid black) and a QD (solid blue).

highly excited hole states). The size of the dots indicates the optical intensity, estimated within the dipolar approach [22]. One can see that the theory captures qualitatively the magnetic response observed in Fig. 3, with a moderate diamagnetic shift of the GS transitions and a larger, nonlinear paramagnetic shift of the optically active ES1 transitions.

As evident in Fig. 5(a), it is straightforward to identify the quadratic-in- $B$  term,  $H_e^{B^2}$ , as the origin of the diamagnetic shift with increasing field in GS shells because  $L_z = 0$  in circular symmetry and the linear-in- $B$  terms in Eq. (2) vanish. In contrast, for ES1 states  $H_e^{B^2}$  is necessarily positive and  $L_z$  is not well defined. There are two factors potentially responsible for the paramagnetic (red) shift of ES1: (1) an enhancement of the electron-hole Coulomb interaction,  $V_{eh}$ , as the increasing magnetic field localizes the electron into the same QD as the hole and (2) the linear-in- $B$  single-particle terms,  $H^{B^1} = H_e^{B^1} + H_h^{B^1}$ . To identify the physical origin of the paramagnetic shift we compare the expectation value of these two terms for the optically active ES1 exciton. The results, displayed in Fig. 5(b), clearly show that  $\langle V_{eh} \rangle$  has a slight blueshift and the net redshift originates in the  $H^{B^1}$  term.

## VI. DISCUSSION

The above result is somewhat surprising in two senses. First, the Coulomb attraction gives no contribution to the paramagnetic shift (rather the opposite) in spite of  $B$  driving the electron and hole into the same QD. This is because the field lifts exciton quasidegeneracies, thus reducing Coulomb correlations that helped increase electron-hole attraction. Second, it is not obvious that  $H^{B^1}$  should give a redshift in an LQDM.  $H^{B^1}$  does induce a redshift in single QDs with nearly circular symmetry [28], but in such a case  $L_z$  is a good quantum number and the optically active  $p$ -shell exciton is mainly formed by an electron with  $L_z^e = -1$  and a hole with  $L_z^h = +1$ . Both  $H_e^{B^1}$  and  $H_h^{B^1}$  contribute to the exciton redshift in a single QD, though  $H_e^{B^1}$  is primarily responsible due to the lighter electron mass. In a LQDM, however, the symmetry is drastically lowered and the states have no well-defined  $L_z$ . One may then expect  $\langle L_z^e \rangle \approx 0$ , which would suppress the paramagnetic shift, but we find exactly the opposite behavior. If we compare the redshift induced by  $\langle H^{B^1} \rangle$  for the LQDM and one of the constituent QDs alone [see Fig. 5(b)], the former is twice larger. In a single QD,  $\langle L_z^e \rangle$  smoothly decreases from 0 to  $-1$  atomic units as the magnetic field  $B$  increases (see red dots in Fig. 6). In contrast,  $\langle L_z^e \rangle$  in the quasidegenerate LQDM fluctuates and evolves from 0 towards negative values well under  $-1$  (see blue dots in the figure). As a consequence, ES1 in the LQDM shows a pronounced redshift. The overall redshift is similar for single QD and LQDM because other terms like  $H_e^{B^2}$  compensate.

This behavior is explained as follows. The  $B$ -induced carrier localization into the QDs makes the LQDM emission spectrum resemble that of two individual, nearly degenerate QDs (cf. Fig. 5 with Fig. 2 of Ref. [32]). At the same time, the lowered symmetry enables mixing between states which would otherwise have different  $L_z$ . In particular, for the electron it allows strong mixing between the states that eventually converge to the lowest Landau level, which in the single QD would have  $L_z^e \leq 0$ . As a result,  $\langle L_z^e \rangle$  rapidly decreases with  $B$ .

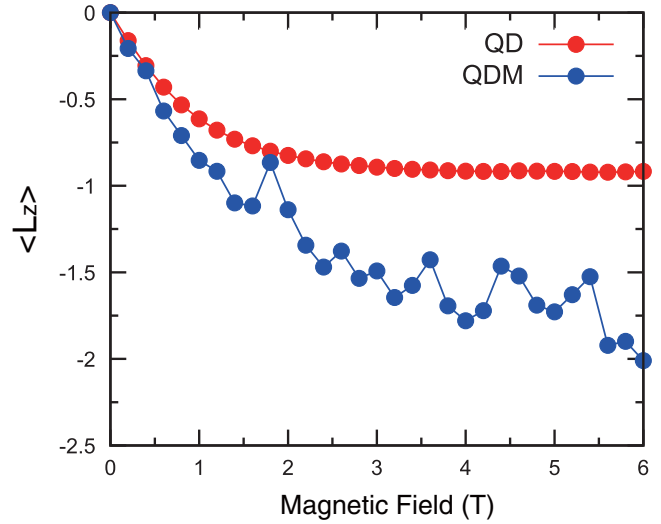


FIG. 6. (Color online) Angular momentum expectation value for the electron in a  $p$ -shell exciton of a single QD (red dots) and that of a quasidegenerate LQDM (blue dots). For the single QD  $\hbar\omega = 25$  meV. For the LQDM  $\hbar\omega_L = 23.5$  meV (left dot) and  $\hbar\omega_R = 25.0$  meV (right dot). The distance between QD centers is 35 nm.

The high areal density of LQDMs in our sample makes it impossible to conclusively assign ES1 PL to a LQDM with degenerate vs nondegenerate GS energies of the two constituent QDs. However, we can use theoretical models to estimate the influence of changing degeneracy. Figure 7 shows the calculated exciton emission spectrum and exciton charge densities of LQDMs with different interdot spacing and degrees of degeneracy under magnetic field. Red dots are used to highlight the molecular exciton state. Although the spatial localization of charges in ES1 depends strongly on the inter-QD degeneracy, no significant change in the paramagnetic energy shifts is observed. The nondegenerate LQDMs can be considered as a system with properties between a single QD and a LQDM with nearly degenerate constituent QDs. In nondegenerate LQDMs the increase of the angular momentum with increasing magnetic field is weaker than in quasidegenerate LQDMs while the Coulomb attraction increases more quickly. The net effect of these two factors leads to a 5 meV energy shift when  $B = 6$  T regardless of the degree of degeneracy.

In conclusion, we used PL measurements of single LQDMs to observe the energy shift of discrete states as a function of applied magnetic field in the Faraday configuration. The redshift in the energy of first excited states is comparable to that observed for single QDs despite the broken circular symmetry of the LQDMs. We show that this redshift arises due to a competition between two effects: (1) the magnetic field localizes molecular states into the individual dots where coupling between states of the lowest Landau level leads to a significant increase of the angular momentum and a large redshift in state energy, and (2) the magnetic field splits exciton states energetically, thus reducing Coulomb correlations and offsetting the large redshift due to the angular momentum term. The fact that the molecular character of ES1 states can be switched on and off with applied magnetic fields, which cannot

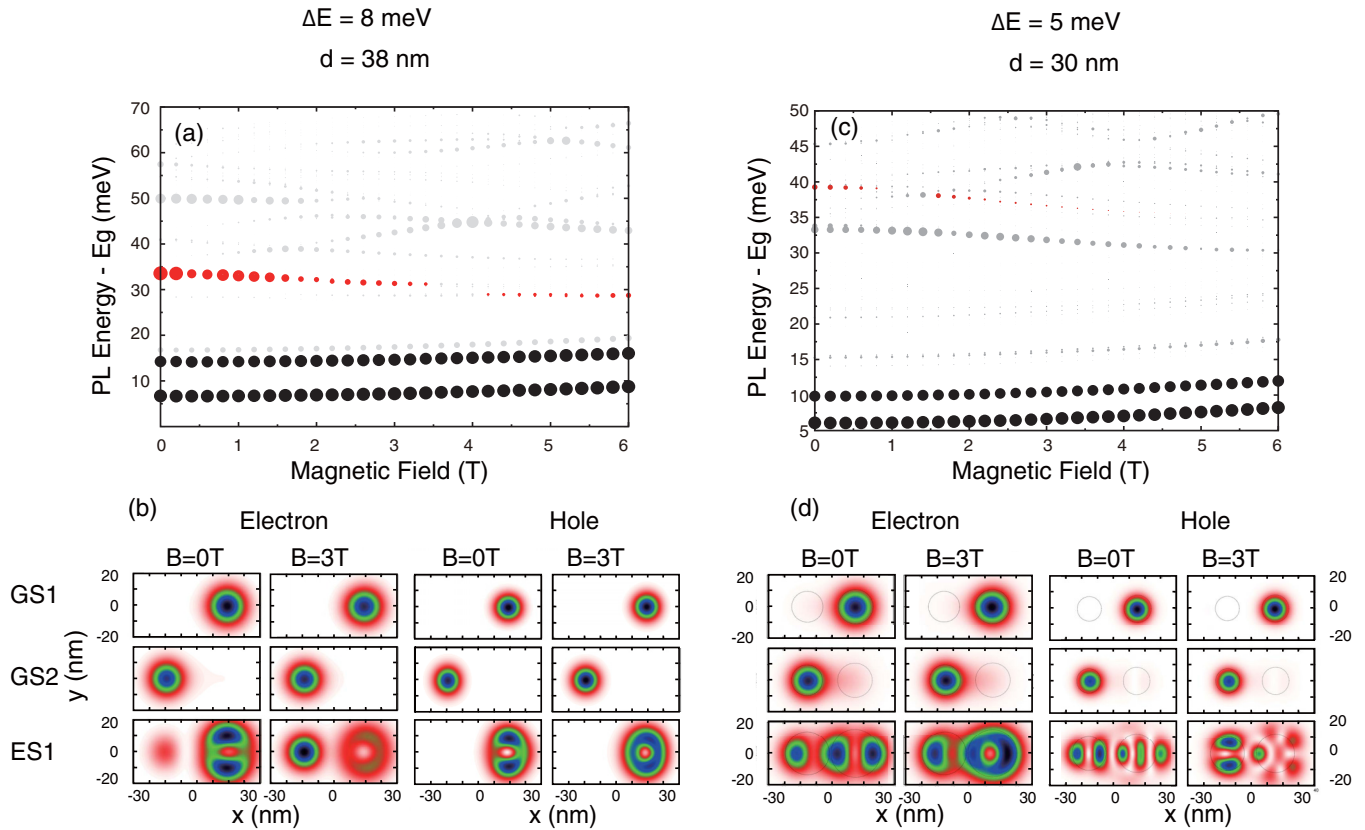


FIG. 7. (Color online) Calculated exciton emission spectra (top row) and exciton charge densities (bottom row) of LQDMs with different degrees of degeneracy.

be observed in single QDs or VQDMs, suggests that there may be new opportunities for manipulating the spatial extent of wave functions and coherent interactions between isolated quantum states. The results further suggest that the structural symmetry of QD molecules can be manipulated to tailor the optoelectronic and quantum properties of QD materials for next-generation device applications.

#### ACKNOWLEDGMENTS

We thank J. Planelles for helpful discussions. The work was financially supported by NSF DMR-0844747 (X.Z., M.D.), APOSTD/2013/052 GV VALi+d Grant (M.R.), NRF of Korea No. 2011-C0030821/2013R1A1A1007118 (J.L.), NSF DMR 1309989 (G.S.), and MINECO Project No. CTQ2011-27324 (J.I.C.).

- [1] A. J. Shields, *Nat. Photon.* **1**, 215 (2007).
- [2] R. J. Warburton, *Nat. Mater.* **12**, 483 (2013).
- [3] S. E. Economou, J. I. Climente, A. Badolato, A. S. Bracker, D. Gammon, and M. F. Doty, *Phys. Rev. B* **86**, 085319 (2012).
- [4] H. J. Krenner, M. Sabathil, E. C. Clark, A. Kress, D. Schuh, M. Bichler, G. Abstreiter, and J. J. Finley, *Phys. Rev. Lett.* **94**, 057402 (2005).
- [5] E. A. Stinaff, M. Scheibner, A. S. Bracker, I. V. Ponomarev, V. L. Korenev, M. E. Ware, M. F. Doty, T. L. Reinecke, and D. Gammon, *Science* **311**, 636 (2006).
- [6] A. S. Bracker, M. Scheibner, M. F. Doty, E. A. Stinaff, I. V. Ponomarev, J. C. Kim, L. J. Whitman, T. L. Reinecke, and D. Gammon, *Appl. Phys. Lett.* **89**, 233110 (2006).
- [7] M. F. Doty, M. Scheibner, I. V. Ponomarev, E. A. Stinaff, A. S. Bracker, V. L. Korenev, T. L. Reinecke, and D. Gammon, *Phys. Rev. Lett.* **97**, 197202 (2006).
- [8] H. J. Krenner, E. C. Clark, T. Nakaoka, M. Bichler, C. Scheurer, G. Abstreiter, and J. J. Finley, *Phys. Rev. Lett.* **97**, 076403 (2006).
- [9] M. F. Doty, M. Scheibner, A. S. Bracker, I. V. Ponomarev, T. L. Reinecke, and D. Gammon, *Phys. Rev. B* **78**, 115316 (2008).
- [10] M. F. Doty, J. I. Climente, M. Korkusinski, M. Scheibner, A. S. Bracker, P. Hawrylak, and D. Gammon, *Phys. Rev. Lett.* **102**, 047401 (2009).
- [11] L. Wang, A. Rastelli, S. Kiravittaya, M. Benyoucef, and O. G. Schmidt, *Adv. Mater.* **21**, 2601 (2009).
- [12] W. Liu, S. Sanwlani, R. Hazbun, J. Kolodzey, A. S. Bracker, D. Gammon, and M. F. Doty, *Phys. Rev. B* **84**, 121304 (2011).
- [13] W. Liu, A. S. Bracker, D. Gammon, and M. F. Doty, *Phys. Rev. B* **87**, 195308 (2013).
- [14] X. Zhou, S. Sanwlani, W. Liu, J. H. Lee, Z. M. Wang, G. Salamo, and M. F. Doty, *Phys. Rev. B* **84**, 205411 (2011).
- [15] X. R. Zhou, J. H. Lee, G. J. Salamo, M. Royo, J. I. Climente, and M. F. Doty, *Phys. Rev. B* **87**, 125309 (2013).
- [16] G. Beirne, C. Hermannstadter, L. Wang, A. Rastelli, O. Schmidt, and P. Michler, *Phys. Rev. Lett.* **96**, 137401 (2006).

- [17] X. Zhou and M. Doty, *J. Appl. Phys.* **116**, 163101 (2014).
- [18] C. Hermannstadter, G. J. Beirne, M. Witzany, M. Heldmaier, J. Peng, G. Bester, L. Wang, A. Rastelli, O. G. Schmidt, and P. Michler, *Phys. Rev. B* **82**, 085309 (2010).
- [19] J. Peng, C. Hermannstadter, M. Witzany, M. Heldmaier, L. Wang, S. Kiravittaya, A. Rastelli, O. G. Schmidt, P. Michler, and G. Bester, *Phys. Rev. B* **81**, 205315 (2010).
- [20] J. Peng and G. Bester, *Phys. Rev. B* **82**, 235314 (2010).
- [21] G. Munoz-Matutano, M. Royo, J. I. Climente, J. Canet-Ferrer, D. Fuster, P. Alonso-Gonzalez, I. Fernandez-Martinez, J. Martinez-Pastor, Y. Gonzalez, L. Gonzalez *et al.*, *Phys. Rev. B* **84**, 041308 (2011).
- [22] M. Royo, J. I. Climente, and J. Planelles, *Phys. Rev. B* **84**, 235312 (2011).
- [23] M. Heldmaier, M. Seible, C. Hermannstädter, M. Witzany, R. Rossbach, M. Jetter, P. Michler, L. Wang, A. Rastelli, and O. G. Schmidt, *Phys. Rev. B* **85**, 115304 (2012).
- [24] J. Lee, Z. Wang, V. Dorogan, Y. Mazur, and G. Salamo, *IEEE Trans. Nanotechnol.* **9**, 149 (2010).
- [25] S. Brown, T. Kennedy, D. Gammon, and E. Snow, *Phys. Rev. B* **54**, R17339 (1996).
- [26] H. Kim, T. C. Shen, D. Sridharan, G. S. Solomon, and E. Waks, *Appl. Phys. Lett.* **98**, 091102 (2011).
- [27] M. Bayer, A. Schmidt, A. Forchel, F. Faller, T. L. Reinecke, P. A. Knipp, A. A. Dremin, and V. D. Kulakovskii, *Phys. Rev. Lett.* **74**, 3439 (1995).
- [28] S. Raymond, S. Studenikin, A. Sachrajda, Z. Wasilewski, S. J. Cheng, W. Sheng, P. Hawrylak, A. Babinski, M. Potemski, G. Ortner *et al.*, *Phys. Rev. Lett.* **92**, 187402 (2004).
- [29] S. Hameau, Y. Guldner, O. Verzelen, R. Ferreira, G. Bastard, J. Zeman, A. Lemaitre, and J. M. Gerard, *Phys. Rev. Lett.* **83**, 4152 (1999).
- [30] F. Gagel and K. Maschke, *Phys. Rev. B* **52**, 2013 (1995).
- [31] Y. Sidor, B. Partoens, F. M. Peeters, N. Schildermans, M. Hayne, V. V. Moshchalkov, A. Rastelli, and O. G. Schmidt, *Phys. Rev. B* **73**, 155334 (2006).
- [32] U. Hohenester and E. Molinari, *Phys. Status Solidi A* **178**, 277 (2000).
- [33] See <https://code.google.com/p/citool/>